Power Coupling Between Light Diffusing Fibers: Modelling and Validation

Pasquale Imperatore, *Member, IEEE*, Genni Testa, Gianluca Persichetti, and Romeo Bernini, *Member, IEEE*

***Abstract*—The power coupling between two light diffusing multimodal optical fibers of equal and finite lengths that are parallel oriented, and which are coupled through scattering processes, is investigated both theoretically and experimentally. In particular, a simple analytical model of the inherent coupling coefficient, derived according to a perturbation approach in a weak-coupling regime, is developed. The modelling results have been compared with the measurements performed, as a function of fiber distance and coupling length at three different wavelengths, and a close agreement is proved. The obtained results provide a better understanding of the power coupling mechanism and of the inherent functional dependence on the main structural parameters of the two-fiber configuration.**

***Index Terms*—Light diffusing fiber, perturbation models, power coupling, radiometry, scattering.**

I. Introduction

LIGHT diffusing optical fibers (LDFs) exploitation is currently of great interest [1]–[5]. These fibers have been designed and employed mainly for lighting or light delivery in biomedical applications [1]–[2]. More recently, these fibers have been used for efficient disinfection [3], for optical communications [4] and sensing applications [5].

In LDF some power from the propagating mode is radiated out through the lateral surface of the fiber by scattering. In particular, the losses are caused by the interaction of light with submicron-sized density fluctuations placed in the core of the fiber. With a suitable design and control of manufacturing process it is possible to obtain a very uniform emission of the propagating light through the side and along the length of the optical fiber.

Up to now, only the out-coupling properties of light diffusing fibers are fully exploited in the proposed applications, whereas the in-coupling functionalities are neglected. Recently, the power coupling between two parallel oriented light-diffusing optical fibers has been used for the development of a continuous liquid level sensor [6].

Typically, in optics, the power coupling is due to the overlap of evanescent-wave (non-radiative) modal fields of two parallel dielectric waveguides in close proximity [7]. This phenomenon has been widely studied [8] and applied in order to develop optical devices and sensors [9]. However, power coupling could be also related to light scattering from waveguide perturbations, controlled or randomly located, causing a radiative process. In this case, the light that is scattered out from the guided mode of one guide can be scattered into the guided mode of a neighboring waveguide. This approach is very interesting and permits power coupling even when the fiber are at a very large distance in terms of wavelength. It is worth emphasizing that coupling, scattering, and reciprocity, are three intimately connected concepts [10].

Marcuse has analyzed the coupling by scattering between slab waveguides due to random core-width variations [11]. Melati *et al.* have reported a comprehensive experimental characterization of optical crosstalk between planar waveguides caused by scattering [12]. Radiatively coupled corrugated waveguides have been also theoretically analyzed [13]. Power coupling in side-emitting optical fibers has been employed in order to develop optical devices for force sensing and optical spectroscopy [14]–[15]. However, an evaluation of the radiative coupling coefficient between two dielectric waveguides and its functional dependence on the structural parameter have not been clearly established yet.

Having at our disposal this information is high desirable, since it provides a better understanding of the power coupling mechanism, thus enabling further developments in application design and optimization of the device performance.

Modeling of the power exchange between two parallel light diffusing fibers has been conducted by using a system of coupled first-order differential equations in [6], [16]. The obtained closed-form solutions, which describe the average power distribution in the fibers for both counter-propagating and co-propagating configurations, provide a good understanding of the dynamic of power coupling at system level.

In this paper, we investigate the power coupling between two parallel oriented light diffusing fibres, both theoretically and experimentally. In particular, the exact analytical treatment might be prohibitive for the canonical configuration under investigation. Nonetheless, in this paper we develop an analytical model of the coupling coefficient, which is carried out according to a perturbative approach and under suitable approximations. Specifically, we develop a simple analytical model of the coupling coefficient in a weak-coupling regime, thus enabling the investigation of the inherent functional dependence on the structural parameters of the two-fiber canonical configuration.

Manuscript received June 24, 2021; revised September 3, 2021 and October 12, 2021; accepted October 13, 2021. Date of publication October 19, 2021; date of current version February 1, 2022. *(Corresponding author: Romeo Bernini.)*

The authors are with the Institute for Electromagnetic Sensing of the Environment (IREA), National Research Council of Italy (CNR), Napoli 80126, Italy (e-mail: imperatore.p@irea.cnr.it; testa.g@irea.cnr.it; persichetti.g@irea.cnr.it; bernini.r@irea.cnr.it).

Color versions of one or more figures in this article are available at https://doi.org/10.1109/JLT.2021.3120865.

Digital Object Identifier 10.1109/JLT.2021.3120865

The proposed model is successfully validated by measuring the power coupling as a function of inter-fiber distance and coupling length, and for three different wavelengths ranging from the visible to the near infrared.

The paper is organized as follows. Section II provides an overview of the existing formalism for describing the power coupled system. The novel model is analytically formulated in Section III. The experimental setup is described in Section IV. The carried out measurements and a pertinent comparative discussion are provided in Section V. Section VI concludes the paper.

II. Power-Coupling Equations

The power coupling between two propagating waves of two multimode fibers, which in our configuration is caused by random imperfections, can formally be described in terms of a first-order system of ordinary differential equations, in the form [6]:

$$\begin{cases} \frac{dP_1}{dx} = -(\alpha+\beta)P_1 + \beta P_2 \\ \frac{dP_2}{dx} = \pm\beta P_1 \mp (\alpha+\beta)P_2 \end{cases} \quad (1)$$

where the upper signs refers to *co-propagating* configuration with the boundary conditions $P_1(0) = P_{in}$ and $P_2(0) = 0$, and the lower signs to the *counter-propagating* configuration with the boundary conditions $P_1(0) = P_{in}$ and $P_2(H) = 0$, and with H denoting the coupling length. In particular, $P_1(x)$ and $P_2(x)$ describe the average power in the illuminating and detection fiber, respectively; x is the distance along the guide; β is the *coupling coefficient*; α is the (power) attenuation coefficient of fibers.

The analytical solutions for both co-propagation and counter-propagation configurations have been established in closed form in [6], thus providing a useful tool. As a result, this formalism represents a rather solid conceptual framework.

Nonetheless, the formal solution of the power coupling equations cannot be completed as the per-unit-length parameters in them are unknown. In particular, the parameters of attenuation, α, and coupling, β, are essential elements in the determination of the power distribution from the solution of power coupling equations. It is important to highlight that these per-unit-length parameters are typically assumed independent of the longitudinal coordinate.

Typically, the fiber attenuation coefficient α includes both absorption and scattering losses in each fiber. However, in light diffusing fiber the absorption losses are negligible compared to the scattering losses, and thus the constant α is mainly attributed to the concentration of scattering particles embedded in the fiber, which cause side-scattering along the fiber. The power emitted from isolated side-scattering fibers was experimentally studied for different fibers and wavelengths [17], [18].

The power coupling by scattering has been investigated theoretically by a one-dimensional model [11] and experimentally in planar geometry [12], but a comprehensive analysis of the radiative coupling between two light-diffusing fibers is still missing.

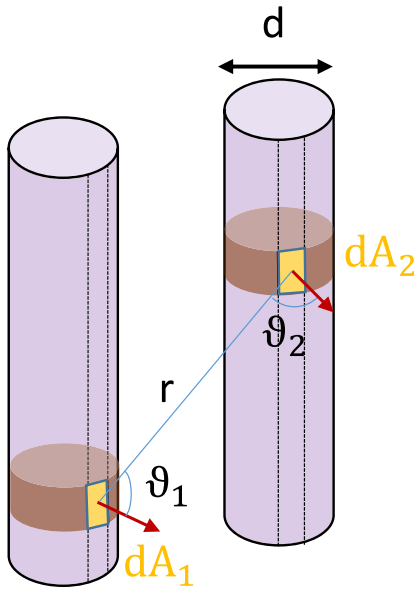

Fig. 1. Geometric scheme: parallel oriented cylindrical fibers of equal and finite lengths.

In order to proceed further, it is useful to provide a more detailed description taking into account how the coupling mechanism parametrically reflects the geometry of the problem, as discussed in the next Section.

III. Analytical Modelling of Coupling Coefficient

The problem at hand involves the power transfer between two parallel oriented, light diffusing cylindrical fibers of equal and finite lengths (Fig. 1). A pertinent rigorous solution of this problem is hard to be analytically obtained without some approximation, especially since the power radiated by the fiber is generally not uniform along the longitudinal extension of the cylinder. As a matter of fact, even in the case of uniform distribution of the radiated power along the cylinder, the problem is amenable to a closed-form solution only in some limiting cases [19].

According to a perturbative approach [20], we first estimate the power irradiated, evaluated in the absence of the detection fiber, by the illuminated fiber and impinging upon the detection fiber (Section III.A). Then the coupling coefficient is evaluated in the first-order limit of the perturbative approach (Section III.B).

As a result, we give an analytical solution to the problem that is valid as the transverse width of the fibers is relatively small with respect to the distance between the two parallel cylinders, which is indeed acceptable for the cases of interest.

A. A Simple Radiant-Power Transfer Model

Let us investigate the power transfer between the parallel fibers of equal diameter d placed at a distance W. We start our analysis by referring to the geometrical scheme depicted in Fig. 1. According to classical radiometry [21], the overall power $d\Phi_{1\to2}$ transferred from the surface area A_1 of the illuminating fiber to the differential area dA_2 centered at the longitudinal

coordinate x_2 on the detecting fiber can be written in the form:

$$d\Phi_{1\to 2}\ (x_2) = \int_{A_1} L_1\,(\mathbf{p})\,\frac{\cos\vartheta_1\cos\vartheta_2}{r^2}dA_2dA_1 \qquad (2)$$

where

- $L_1(\mathbf{p})$ denotes the radiant power per unit area, per unit solid angle and per unit wavelength interval [21];
- the vector $\mathbf{p}$ denotes an arbitrary position along the lateral surface of the illuminating fiber;
- A_1 is the lateral surface of the illuminating fiber;
- r is the length of the line that connects the two elemental areas dA_1 and dA_2, respectively (Fig. 1).

A perfectly diffuse or "lambertian" surface element dA_1 is one for which the (emitted) radiance is isotropic, so that L_1 is a constant regardless the direction. Equation (2) is defined in terms of the cosines of angles between normal directions to these surface area elements and the line r, namely $\cos\vartheta_1$ and $\cos\vartheta_2$, and by the areas, dA_1 and dA_2, of these surface elements.

As finite surface areas of the illuminating fiber are considered, integration in (2) can be very complicated. Conversely, the numerical integration of (2) might be obtained with high accuracy; however, an insight into the functional dependency on the structural parameters in such a way cannot be achieved. Therefore, in the following we focus on the inherent analytical treatment, thus suitably introducing reasonable approximations. In particular, in order to get a treatable analytical expression, we simplify the model according to the scheme depicted in Fig. 2, where the condition $d << W$ is assumed. Specifically, θ denotes the angle between the normal to the surface and the line between the centres of dA_1 and dA_2 (see Fig. 2), thus $\theta = \mathrm{acos}(\frac{W}{r})$. Hence, we reasonably assume that $\vartheta_n \approx \theta$, with $n = 1, 2$. Differently from [6], we here distinguish, for the sake of convenience, the coordinates x_1 and x_2 along the axis of the illuminating and detecting fiber, respectively. The area of the elemental rectangular surface is given by $dA_n = dx_n d$ with $n = 1, 2$ (see Fig. 2).

The distribution of the incident power on the elemental surface area dA_2 of the detection fiber is obtained by integrating (incoherently summing) the power contributions coming from each infinitesimal elements dA_1 of the illuminating fiber.

Although it might appears to be rather drastic, such a simplification is valuable, since it permits to effective model the power exchange in terms of the essential structural parameters, as it will be clear in the following.

By specializing (2), after straightforward manipulations, we obtain the following expression given in convolutional form:

$$d\Phi_{1\to 2}(x_2) = dA_2\pi\left(\frac{d}{2W}\right)\int_0^H L_1\,(x_1)\,K_W(x_2 - x_1)dx_1 \qquad (3)$$

where the upper limit of the integral H represents the coupling length of the fibers (Fig. 2), and the convolutional kernel is given by

$$K_W(x_2 - x_1) = \frac{2}{\pi}\,\frac{W^3}{\left[W^2 + (x_2 - x_1)^2\right]^2} \qquad (4)$$

where W represents indeed a broadening (width) parameter.

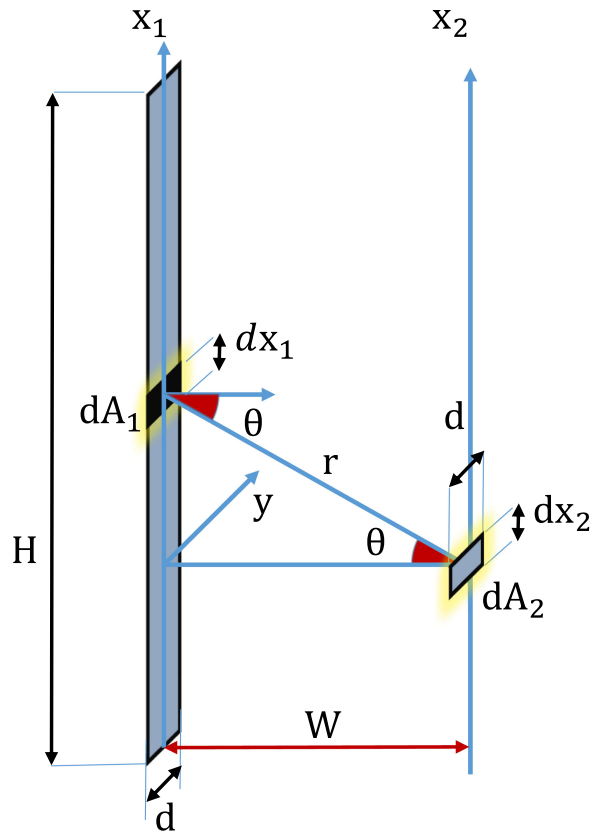

Fig. 2. Simplified Geometric scheme.

The expression (3) can be conveniently rewritten in the form:

$$\frac{d\Phi_{1\to 2}}{dA_2}\ (x_2) = \pi\left(\frac{d}{2W}\right)L_1\,(x_2)\,I\,(x_2, W) \qquad (5)$$

where I describes a dimensionless quantity, defined as:

$$I\,(x_2, W) = \int_0^H \frac{L_1\,(x_1)}{L_1\,(x_2)}K_W(x_2 - x_1)dx_1 \qquad (6)$$

It should be noted that the singly peaked energy distribution $K_w(x)$ appearing in our model formally represents a normalized *squared Lorentzian* function [22], [23]. The full width at half-maximum (FWHM) is given by $2W\sqrt{\sqrt{2}-1} \approx 1.29\,W$. The squared-Lorentzian lineshape for different values of the parameter W is depicted in Fig. 3. It should be emphasized that $K_W(x)$ asymptotically approaches the *Dirac*'s delta function $\delta(x)$ as $W\to 0$. Accordingly, we get $I\,(x_2, 0) = 1$.

An interesting physical interpretation is in order. The expression (3) describes the combined effect of incoherent radiation, coming from the different elements of the illuminating fibers, which contribute to the power per unit area incident on the detecting fiber at the abscissa x_2. Notice that the elementary contribution to the power radiated by the illuminating fiber coming from x_1 that is far from the abscissa x_2 is very small in this convolution.

Therefore, for a prescribed elemental surface area dA_2 of the detecting fiber at x_2, the extension of the illuminating fiber surface essentially contributing to the power-transfer toward the

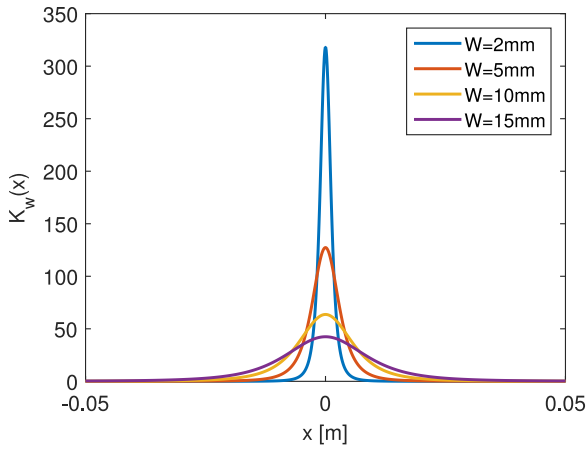

Fig. 3. Squared Lorentzian convolutional kernel $\mathrm{K_W(x)}$.

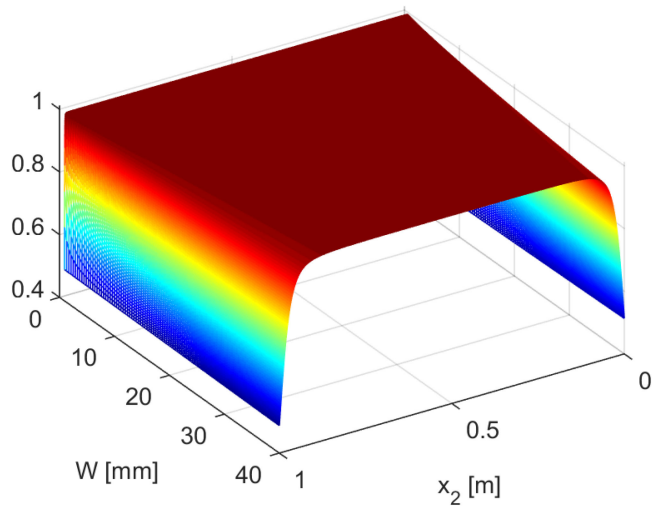

Fig. 4. The function $\mathrm{I(x_2, W)}$, for α=1 and H=1.

differential area $\mathrm{dA_2}$ can be characterized as follows: its *transverse* extension is d, while the corresponding (predominant) *longitudinal* extension is directly proportional to the characteristic broadening parameter W (Fig. 2).

B. Perturbative Approach

The coupling coefficient β cannot be determined exactly, even for the canonical structure considered in this paper. However, its approximated expression is obtained in parametric form in this Section by resorting to a perturbative approach. Therefore, to solve the problem we adopt a perturbative approach [20], which is consistent with the regime of weak coupling. The unperturbed $\mathrm{L_1}$ is therefore obtained by referring to the associated unperturbed configuration, i.e., the illuminating fiber acting in the free space, as described in the following.

The solution of first-order ordinary differential equation describing guided propagation of the average power in the illuminating fiber, in absence of the detecting fiber, referred to as a zero-order solution, is given in the form $\mathrm{P_1^{(0)}(x_1)} = \mathrm{P_1^{(0)}}(0)\exp[-\alpha\, \mathrm{x_1}]$. It describes the (unperturbed) power distribution along the illuminating fiber acting in the free space, with $\mathrm{P_1^{(0)}}(0)$ denoting the input power and α representing the attenuation coefficient of the illuminating fiber. Accordingly, the side-scattering fiber has a constant decay of the illumination (average) power along its working length [24], [25].

It can be useful to provide a description of this coefficient in terms of scattering from a random distribution of particles [26], as follows. Let n be the number of particles per unit volume in the illuminating (or detecting) fiber. Under the independent scattering assumption [26], we get $\alpha = \mathrm{n}\sigma_\mathrm{s}$, where σ_s is the area cross section of a single particle.

The side-scattered power emitted by an element of lateral surface (with longitudinal extension $\mathrm{dx_1}$) of the illuminating waveguide is first concerned. According, the side-emitting (unperturbed) radiance $\mathrm{L_1}$ at the abscissa $\mathrm{x_1}$ can be calculated as [17], [27]:

$$\mathrm{L_1\ (x_1)} = \tau_1 \lim_{\Delta \mathrm{x}\to 0} \frac{\mathrm{P_1^{(0)}\,(x_1) - P_1^{(0)}\,(x_1+\Delta x)}}{2\pi \mathrm{d}\Delta \mathrm{x}}$$

$$= \tau_1 \frac{\alpha\, \mathrm{P_1^{(0)}(x_1)}}{2\pi \mathrm{d}} \tag{7}$$

where $\mathrm{P_1^{(0)}(x_1)}$ denotes the (unperturbed) solution and τ_1 is the transmittance of the lateral surface of the illuminating fiber. It should be noted that the non-uniformity of the side-scattering radiance distribution, $\mathrm{L_1 = L_1\ (x_1)}$, along the illuminating waveguide length reflects the exponential attenuation distribution of the power propagating in the unperturbed waveguide. As a consequence, the normalized radiance in (6) $\mathrm{L_1(x_1)/L_1(x_2)}$ has an exponential distribution. More specifically, $\mathrm{L_1(x_1)/L_1\ (x_2)} = \exp[-\alpha(\mathrm{x_2 - x_1})]$.

The integral in (6) has been evaluated numerically for $\alpha = 1$ and $\mathrm{H} = 1$, and it is shown in Fig. 4 as a function of $\mathrm{x_2}$ and W. As a result, one can verify that, for W within a reasonable range, the function $\mathrm{I(x_2, W)}$ defined in (6) is essentially unitary, as it does not depend on $\mathrm{x_2}$, except near the edges (see Fig. 4). Notice that, near the edges ($\mathrm{x_2}$= 0 or $\mathrm{x_2}$= H) the function $\mathrm{I(x_2,\ W)}$ decreases rapidly as W increases. Therefore, the relevance of the boundary effect also depends on the distance between the fibers W. It is then clear than, for a structure that is ideally infinite along the longitudinal dimension (no boundary effects), the function I merely reduces to a unitary factor. For the sake of convenience, in the following we neglect the boundary-effects. Therefore, by combining (5) and (7), we obtain the power captured by the element (with lateral area $\mathrm{dA_2^e}$) of the detecting fiber as follows

$$\tau_2 \frac{\mathrm{d}\Phi_{1\to 2}}{\mathrm{dA_2}}\,(\mathrm{x_2})\,\mathrm{d\ A_2^e} = \tau_2\,\tau_1 \left(\frac{\alpha}{4\mathrm{W}}\right) \mathrm{P_1^{(0)}(x_2)\ dA_2^e} \tag{8}$$

where τ_2 represents the trasmittance of the lateral surface of the detecting fiber, and $\frac{\mathrm{d}\Phi_{1\to 2}}{\mathrm{dA_2}}$ is the power density impinging upon the detecting fiber at $\mathrm{x_2}$. The expression (8) considers the power intercepted by an *effective* differential area $\mathrm{dA_2^e}$, which can be expressed in the form $\mathrm{d\ A_2^e = f\ d\ A_2 =\ f\ d\ \cdot\ dx_2}$, where f is the fractional area occupied by the particles in the detecting fiber.

In particular, we can write

$$\mathrm{f} = \frac{\sigma_\mathrm{s} \mathrm{n\ dV_2}}{\mathrm{dA_2}} = \frac{\pi}{4}\,\alpha\,\mathrm{d} \tag{9}$$

where n is the number of particles per unit volume in the detection fiber, $\mathrm{d\,A_2} = \mathrm{dx_2 d}$ represents the elemental lateral area, and $\mathrm{dV_2} = \mathrm{dx_2}\pi(\mathrm{d}/2)^2$ is the elemental volume. Note that in the last equality we have taken into account that $\alpha = \mathrm{n}\sigma_\mathrm{s}$ [26].

In the limit of the first-order approximation, the average power $\mathrm{P_2}{=}\mathrm{P_2}\,(\mathrm{x_2})$ propagating in the detecting fiber can be described according to the following equation [see also (1)]:

$$\frac{\mathrm{dP_2}}{\mathrm{dx_2}} = -\tilde{\alpha}\,\mathrm{P_2}\,(\mathrm{x_2}) + \mathrm{s^{(0)}}\,(\mathrm{x_2}) \tag{10}$$

where $\tilde{\alpha}$ represents an equivalent attenuation coefficient of the detecting fiber, and $\mathrm{s^{(0)}}(\mathrm{x_2})$ can be regarded as a spatial varying source impressed along the propagation direction $\mathrm{x_2}$. According to a first-order perturbation development, $\mathrm{s^{(0)}}(\mathrm{x_2})$ can be related to the radiant (unperturbed) power impinging on the lateral surface of the detecting fiber, which is then directed into guided propagation through a scattering processing. The unperturbed power represents the power that would be irradiated by an isolated illuminating fiber.

According to the degree of approximation in (8), $\mathrm{s^{(0)}dx_2}$ can be linked to the fraction of incident radiant power intercepted by the effective area $\mathrm{dA_2^e}$ of the element of detection fiber, as follows

$$\mathrm{s^{(0)}}\,(\mathrm{x_2})\,\mathrm{d\,x_2} = \tau_2\,\frac{\mathrm{d}\Phi_{1\to 2}}{\mathrm{dA_2}}\,(\mathrm{x_2})\,\mathrm{dA_2^e} \tag{11}$$

Noting that formally we have $\mathrm{s^{(0)}}\ (\mathrm{x_2}) = \beta \mathrm{P_1^{(0)}}(\mathrm{x_2})$ [see also (1)], where the coefficient β describes the strength of the coupling between the fibers.

As a result, β can be identified as the *coupling coefficient* between illuminating and detecting fibers. By combining (8)–(11), its expression is established in the form:

$$\beta\ =\ \mathrm{K}\frac{(\alpha\,\mathrm{d})^2}{\mathrm{W}} \tag{12}$$

where, for the sake of conciseness, we have posed $\mathrm{K} = \tau_1\ \tau_2 \pi$ /16.

Therefore, (12) provides a simple formula for the per-unit length coupling coefficient. Remarkably, the larger the power radiated by the illuminated fiber (which is proportional to α) , the greater β. Furthermore, the larger the effective area, which is proportional to αd, intercepting the power radiated by the illuminating fiber, the greater β. Lastly, the coupling coefficient turns out to be proportional to the geometrical factor $\frac{\mathrm{d}}{\mathrm{W}}$.

It is worth noting that (12) is symmetric with respect to the exchange of the roles of illuminating and detecting fiber.

Finally, it is worth emphasizing that the adopted first-order approximation of the perturbative development is consistent with a weak coupling regime ($\beta \ll 1$). Otherwise, multiple interactions between the parallel fibers must be taken into account [20]. The obtained solution is simple and exhibits a direct functional dependence on the main structural parameters. Moreover, it is corroborated by experimental data (as it will be discussed in Section IV), thus effectively capturing the underlying dynamics of the power exchange.

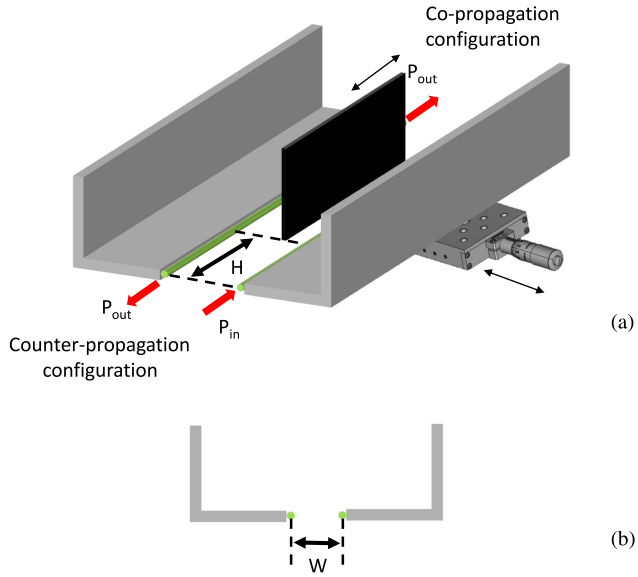

Fig. 5. (a) Experimental setup scheme. (b) section view of the fiber coupling geometry.

IV. Experimental Setup

The experimental setup has been assembled using two light diffusing fibers Fibrance with FC/PC connectors by Corning. Fibrance is a glass fiber in which a section of the core contains a ring of non-periodically distributed (radially and axially) scattering sights with a wide range of sizes (50–500 nm) and lengths (10–1000 mm) [1]. Due to this design, it works as a cylindrical diffuser that emits light uniformly over 360° around the circumference of the fiber. Along the fiber length, the viewing angle, defined as the angle at which the luminance is greater than 50% of the maximum, is >120° and the fiber could be assumed as a Lambertian diffuser. This fiber is characterized by a diffusion length, defined as the distance over which 90 percent of laser light is diffused through side emission. Two Fibrance fibers with a diffusion length of 1m have been used in this work. The fiber has a core diameter of 170 ± 3 μm and a low-index polymeric cladding with a diameter of 230 ± 10 μm [28]. The fiber is protected by a loose tube Polyvinyl Chloride (PVC) jacket with an outer diameter of 900 μm. The experimental setup is depicted in figure Fig. 5.

The two fibers are glued on the edges of two L-shaped aluminium bars (25 × 25 × 1000 mm) (Fig. 2). One of the bar is fixed, whereas the other one is mounted on a precision translation stage that allow a fine control of the distance, W, between the fibers. The L-shaped profile is covered with black masking tape to minimize unwanted light reflections. Due to fiber light diffusing properties, the alignment between the fibers is not critical and it does not requires complex multi-axis stages.

In order to change the coupling length H between the fibers, a black, polyurethane-coated nylon fabric (thickness 0.12 mm) is inserted between the fibers (Fig. 5(a)).

Three fiber coupled laser diodes (LD) at 1550 nm, 976 nm, and 520 nm are employed as light sources, with FC/PC connectors and an output power of about 15 mW. Two different high

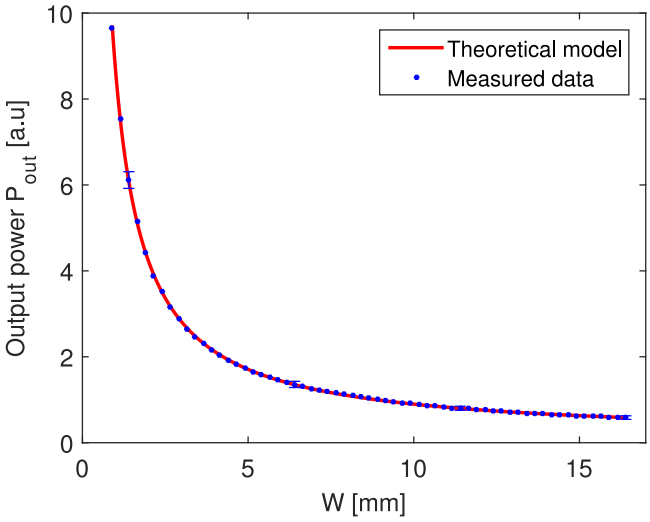

Fig. 6. Output power vs. inter-fiber distance W: comparison between experimental and theoretical results with the co-propagation configuration.

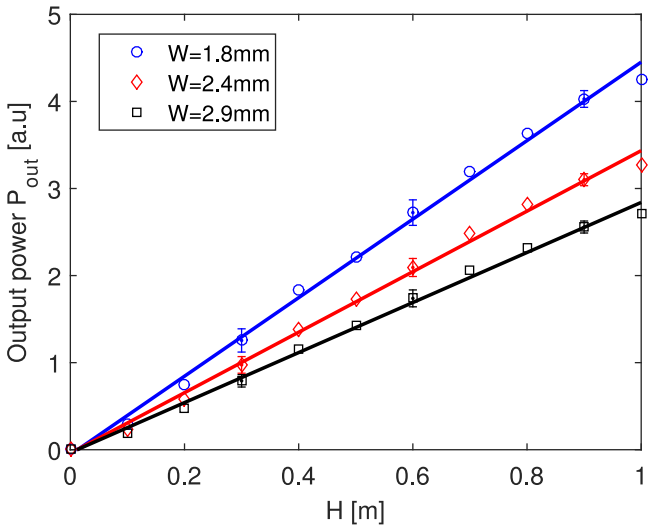

Fig. 7. Output power as a function of the coupling length H, and for different values of the inter-fiber distance W: comparison between experimental and theoretical results with the co-propagation configuration.

sensitivity photoreceivers (PD) are used for light detection. At infrared wavelengths (1550 nm, 976 nm) a Thorlabs PDF10C with a NEP = 7.5 fW/$\sqrt{\text{Hz}}$ and a bandwidth of 25Hz is employed, whereas in the visible region (520 nm) a NewFocus 2151 with a NEP = 16 fW/$\sqrt{\text{Hz}}$ and a bandwidth of 750Hz is adopted.

The photoreceiver voltage output is digitalized with an analog-to-digital converter module connected to a personal computer used for acquire the output power of the detection fiber. All the experiments are conducted by shielding the sensor from ambient light using a black curtain.

The fiber attenuation of the employed fiber at 1550 nm, 976 nm, and 520 nm, has been evaluated by side-scattering technique [29], [30], resulting in the estimated values of 0.86 $\pm$ 0.04 m^{-1}, 1.46 $\pm$ 0.01 m^{-1}, and 1.86 $\pm$0.03 m^{-1} respectively.

V. Results and Discussion

The measurements have been performed at three different wavelengths of 1550 nm, 976 nm, and 520 nm. The distance between the fibers, W, is increased at step of 0.250 mm, from 0.9 mm up to 16 mm. The coupling length, H, between the fibers has been changed in the range 0–1 [m] at step of 0.1 m. The results have been analysed by using a least-squares regression in which the experimental data have been fitted to the theoretical model developed in Section III, as a function of the inter-fiber distance, the coupling length, and the fiber attenuation for the different wavelengths under analysis. The goodness of the fitting procedure and parameters has been evaluated by computing the coefficient of determination R^2.

A. Co-Propagation Configuration

The output power measured in the co-propagation configuration, at $\lambda = 1550$ nm, is shown as a function of the fiber distance W in Fig. 6, also including the error bars. As can be observed, when the distance between the fibers increases, the output power decreases non-linearly. According to the results obtained in [6] and the coupling model developed in Section IV, the output power P_{out}, for $\beta \ll 1$, can be expressed as:

$$\text{P}_{\text{out}} \approx \text{P}_{\text{in}}\beta\text{H} = \text{P}_{\text{in}}\text{K}\frac{(\alpha\text{d})^2}{\text{W}}\text{H} \tag{13}$$

The comparison of measured data with the results obtained via the theoretical model in (13) is illustrated in same figure. As can be observed, the experimental data are well described by the analytical model. The quality of fit of the model has been evaluated by the coefficient of determination R^2, which has been found to be 0.9999, thus indicating that 99.99% of the variability in the response might be explained by the model.

The output power measured as a function of the coupling length H is reported, including the error bars, in Fig. 7, for three different values (1.8, 2.4, and 2.9 mm) of the inter-fiber distance W. As predicted by the model, the coupled power is directly proportional to the coupling length, for a prescribed inter-fiber distance.

Also in this case the quality of the fit of the model is good and R^2 is equal to 0.9953. The measurements have been repeated at 976 nm and 520 nm with the same results, thus confirming that the output power is inversely proportional to the inter-fiber distance W and linearly related to the coupling length H, for a fixed fiber attenuation.

B. Counter-Propagation Configuration

The measurements have been performed also for the counter-propagation configuration. In Fig. 8, the output power measured in this configuration at $\lambda = 1550$ nm is reported as a function of the inter-fiber distance W, including the error bars. In this case

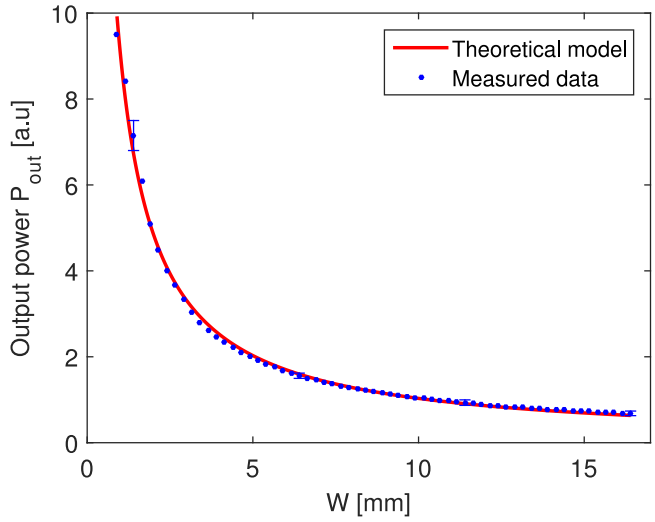

Fig. 8. Output power vs. inter-fiber distance W: comparison between experimental and theoretical results with the counter-propagation configuration.

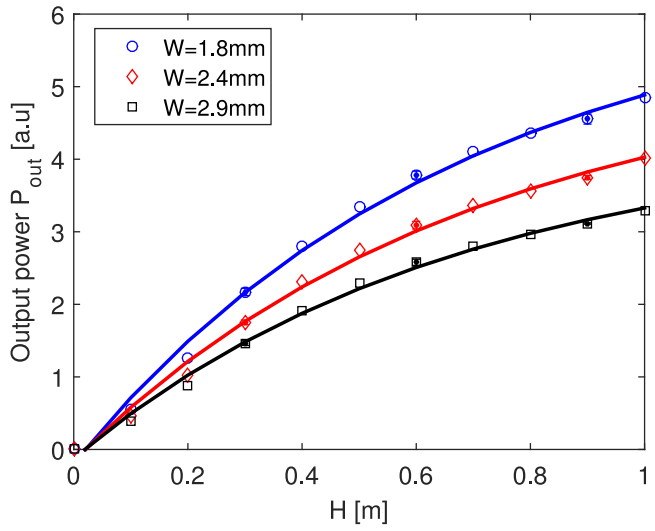

Fig. 9. Output power as a function of the coupling length H, and for different values of the inter-fiber distance W: comparison between experimental and theoretical results in the counter-propagation configuration.

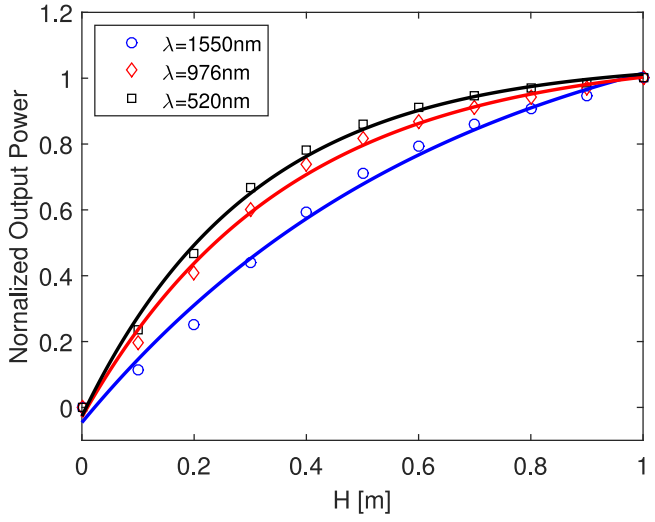

Fig. 10. Normalized output power as a function of the coupling length H, and for different working wavelengths: comparison between experimental and theoretical results in the counter-propagation configuration.

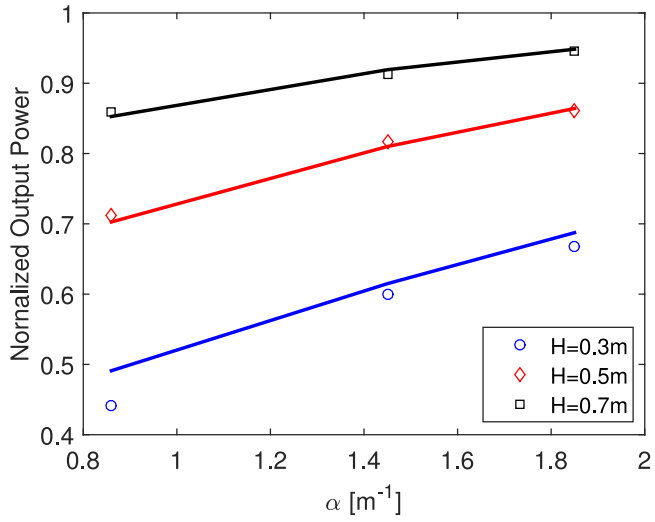

Fig. 11. Normalized output power as a function of the attenuation coefficient α, and for different coupling lengths: comparison between experimental and theoretical results in the counter-propagation configuration.

the output power $\mathrm{P_{out}}$ can be expresses, for $\beta \ll 1$, as [6]:

$$\mathrm{P_{out}} \approx \frac{\mathrm{P_{in}}\beta}{\alpha\left(1+\coth\left[\alpha \mathrm{H}\right]\right)} = \mathrm{P_{in}K}\frac{\alpha \mathrm{d}^2}{\mathrm{W}}\frac{1}{1+\coth\left[\alpha \mathrm{H}\right]} \tag{14}$$

Also in this case the output power is inversely proportional to the fiber distance, and there is a good agreement between the model and the measurement data, as reported in Fig. 8. In this case, R^2 is 0.9964, thus confirming the quality of the fit of the model. The measured output power as a function of the coupling length H is reported in Fig. 9, including the error bars, for three different values of the inter-fiber distance W: 1.8, 2.4, and 2.9 mm. In this case, $\mathrm{P_{out}}$ is non-linearly related to the coupling length. The comparison of the measured data with the theoretical model (14) shows a good agreement ($R^2 = 0.9945$), and the estimated attenuation resulting from the fitting is $\alpha = 0.73 \pm 0.02$ m^{-1}, in accordance with the value measured by side scattering technique.

The measurements have been repeated at 976 nm and 520 nm. In Fig. 10, the comparison of the normalized output power obtained for the different measurement wavelengths is depicted. The non-linear behaviour is more pronounced as the wavelength decreases due to the increase in the attenuation coefficient α, in agreement with (14). The attenuation coefficients resulting from the fitting are $\alpha = 1.33 \pm 0.07$ m^{-1} at 976 nm and $\alpha = 1.62 \pm 0.05$ m^{-1} at 520 nm. These values are in good agreement with the values reported in Section IV.

Finally, the normalized output power as a function of the attenuation coefficient α is reported in Fig. 11, for different coupling lengths H: 0.3 m, 0.5 m and 0.7 m. In Fig. 11 is

also reported the behavior predicted by the theoretical model (continuous line) that is in good agreement with the experimental data.

VI. Conclusion

This study was aimed at investigating the power-coupling between two light-diffusing optical fibers due to the power radiative transfer. In a weak-coupling regime, a simple analytical model of the coupling coefficient has been derived, thus highlighting the functional dependence on the structural basic parameters of the two-fiber system. The experimental results, which are performed by measuring the power coupling as a function of inter-fiber distance and coupling length at different wavelengths, for both the co-propagation and counter-propagation configuration, confirm the validity of the model. These measurements, performed at three different wavelengths ranging from the visible to the IR, show that the coupling efficiency is inversely proportional to the distance between the fibers and it increases at shorter wavelengths due to the increase of the scattering intensity. Differently from the convectional evanescent coupling, the coupling strength is much lower, but the proposed approach allows the coupling also at distances that are very large compared to the working wavelengths and covers a very large wavelength range (1000 nm) that are unachievable with evanescent coupling. The model developed in this paper might be useful in different applications involving coupled diffusing fibers, like liquid level sensing [6], force sensors [14] and optical spectroscopy [15], because its analytical form provides the rationale for optimizing the parameters of the two-fibers configuration. In particular, the operational and structural parameters (e.g., wavelength, inter-fiber distance) of the liquid lever sensor based on coupled light diffusing fibers developed in [6] can be optimized according to the analytical expressions developed in this paper, thus providing a direct example of how the proposed model can be used.

References

[1] S. Logunov, E. Fewkes, F. Shustack, and F. Wagner, "Light diffusing optical fiber for illumination," in *Proc. Renew. Environ. OSA Technical Digest*, Opt. Soc. Amer., Washington, DC, USA, 2013, Paper DT3E.4.

[2] W. S. Klubben *et al.*, "Novel light diffusing fiber for use in medical applications," in *Proc. SPIE 9702, Opt. Fibers Sensors Med. Diagnost. Treat. Appl. XVI*, 2016, p. 970218.

[3] C. Shehatou, S. L. Logunov, P. M. Dunman, C. G. Haidaris, and W. S. Klubben, "Characterizing the antimicrobial properties of 405 nm light and the corning light-diffusing fiber delivery system," *Lasers Surg. Med.*, vol. 51, no. 10, pp. 887–896, 2019.

[4] S. R. Teli, K. Eollosova, S. Zvanovec, Z. Ghassemlooy, and M. Komanec, "Optical camera communications link using an LED-coupled illuminating optical fiber," *Opt. Lett.*, vol. 46, no. 11, pp. 2622–2625, 2021.

[5] N. Cennamo *et al.*, "Biosensors exploiting unconventional platforms: The case of plasmonic light-diffusing fibers," *Sens. Actuators B Chem.*, vol. 337, no. 15, 2021, Art. no. 129771.

[6] P. Imperatore, G. Persichetti, G. Testa, and R. Bernini, "Continuous liquid level sensor based on coupled light diffusing fibers," *IEEE J. Sel. Topics Quantum Electron.*, vol. 26, no. 4, pp. 1–8, Jul./Aug. 2020, Art. no. 5600408.

[7] D. Marcuse, *Theory of Dielectric Optical Waveguides*, 2nd ed. New York, NY, USA: Academic, 1991.

[8] W.-P. Huang, "Coupled-mode theory for optical waveguides: An overview," *J. Opt. Soc. Amer. A*, vol. 11, no. 3, pp. 963–983, 1994.

[9] E. Udd and W. B. Spillman, *Fiber Optic Sensors: An Introduction For Engineers and Scientists*, 2nd ed. New York, NY, USA: Wiley, 2011.

[10] P. Imperatore, A. Iodice, and D. Riccio, "Reciprocity, coupling and scattering: A new look at SPM for rough surface," in *Proc. Eur. Microw. Conf. (EuMC)*, Rome, Italy, 2009, pp. 994–997.

[11] D. Marcuse, "Crosstalk caused by scattering in slab waveguides," *Bell System Tech. J.*, vol. 50, no. 6, pp. 1817–1831, 1971.

[12] D. Melati, F. Morichetti, G. G. Gentili, and A. Melloni, "Optical radiative crosstalk in integrated photonic waveguides," *Opt. Lett.*, vol. 39, no. 13, pp. 3982–3985, 2014.

[13] V. A. Sychugov, A. V. Tishchenko, and B. A. Usievich, "Radiatively coupled corrugated waveguides," *Quantum Electron.*,vol. 24, no. 5, pp. 442–444, 1994.

[14] C. A. Bunge *et al.*, "Textile multitouch force-sensor array based on circular and non-circular polymer optical fibers," *IEEE Sensors J.*, vol. 20, no. 14, pp. 7548–7555, Jul. 2020, doi: 10.1109/JSEN.2020.2985328.

[15] C. O. Egalon, M. P. Matta, D. C. L. Michael, R. Y. Insley, C. C. Jaring, and M. F. Quiday, "Side illuminated optical fiber as a multiplexing element for spectroscopic systems," *Proc. SPIE*, vol. 8847, 2013, Art. no. 88470I.

[16] P. Imperatore, G. Persichetti, G. Testa, and R. Bernini, "Light diffusing fibers for liquid level sensing," *Proc. SPIE*, vol. 11773, 2021, Art. no. 117730W.

[17] M. Zajkowski, "Emission of flux light in 'side light' fiber optic," *Proc. SPIE*, vol. 5125, pp. 322–327, 2003.

[18] A. Endruweit *et al.*, "Spectroscopic experiments regarding the efficiency of side emission optical fibres in the UV-A and visible blue spectrum," *Opt. Lasers Eng.*, vol. 6, no. 2, pp. 97–105, 2008.

[19] N. H. Juul, "View factors in radiation between two parallel oriented cylinders of finite lengths," *J. Heat Transfer*," vol. 104, no. 2, pp. 384–388, 1982.

[20] P. Imperatore, A. Iodice, and D. Riccio, "Second-Order volumetric-perturbative reciprocal scattering theory," *IEEE Trans. Antennas Propag.*, vol. 60, no. 3, pp. 1505–1520, Mar. 2012.

[21] F. Grum and R. J. Becherer, "Optical radiation measurements. vol. 1-Radiometry," Academic, New York, 1979.

[22] G. V.Smirnov, A. I. Chumakov, V. B. Potapkin, R. Rüffer, and S. L. Popov, "Multispace quantum interference in a 57 Fe synchrotron Mössbauer source," *Phys. Rev. A*, vol. 84, no. 5, 2011, Art. no. 053851.

[23] C. Prescher, C. McCammon, and L. Dubrovinsky, "MossA: A program for analyzing energy-domain Mössbauer spectra from conventional and synchrotron sources," *J. Appl. Crystallogr.,* vol. 45, no. 2, pp. 329–331, 2012.

[24] D. Křemenáková, B. Meryová, J. Militký, and V. Lédl, "Illumination intensity changes of side emitting optical fibers," *World J. Eng.*, vol. 10, no. 3, pp. 217–222, 2013.

[25] M. Zajkowski, "Luminous flux emission calculation analysis in side light illumination optical fibres," *Proc. SPIE*, vol. 5775. pp. 440–445, 2005.

[26] T. Leung, J. A. Kong, and K.-H. Ding, *Scattering of Electromagnetic Waves: Theories and Applications*. Hoboken, NJ, USA: Wiley, 2004.

[27] J. Spigulis, D. Pfafrods, M. Stafekis, and W. Jelinska-Platace, "Glowing optical fibre designs and parameters," *Proc. SPIE*, vol. 2967, pp. 231–236, 1997.

[28] "Corning Fibrance light diffusing fiber 2," specification datasheet. [Online]. Available: https://www.corning.com/media/worldwide/Innovation/documents/Fibrance/Corning_Fibrance_Light_Diffusing_Fiber2_%20FINAL_1.9.20.pdf

[29] S. Satoh, K. Susa, and I. Matsuyama, "Simple method of measuring scattering losses in optical fibers," *Appl. Opt.*, vol. 38, no. 34, pp. 7080–7084, 1999.

[30] S. R. Sandoghchi *et al.*, "Optical side scattering radiometry for high resolution, wide dynamic range longitudinal assessment of optical fibers," *Opt. Exp.*, vol. 23, no. 21, pp. 27960–27974, 2015.

Pasquale Imperatore (Member, IEEE) received the Laurea degree (*summa cum laude*) in electronic engineering and the Ph.D. degree in electronic and telecommunication engineering from the University of Naples Federico II, Italy. He is a Research Scientist with National Research Council (CNR), Institute for electromagnetic sensing of the environment (IREA), Naples, Italy. His research interests include electromagnetics and microwave remote sensing, with particular emphasis on theoretical models, scattering in random layered media, synthetic aperture radar (SAR) data modeling and processing, SAR interferometry, parallel algorithms and high performance computing (HPC). He acts as a Reviewer for several peer-reviewed journals. Moreover, he has co-edited two books in the field of remote sensing and geospatial technology.

Genni Testa received the Laurea degree (*summa cum laude*) in solid states physics from the University of Naples Federico II, Naples, Italy, in 2005, and the Ph.D. degree in electrical engineering from the Second University of Naples, Aversa, Italy, in 2008. She is currently a Researcher with the Institute for the electromagnetic sensing of the environment (IREA) of the Italian National Research council (CNR). She is authored or coauthored of more than 30 international journal papers and acts as a reviewer of several international journals. Her research activities include the design, fabrication and characterization of microfluidic and optofluidic devices for biosensing and environmental applications.

Gianluca Persichetti received the Laurea degree in physics from the University of Naples Federico II, Naples, Italy, in 2003 and the Ph.D. degree in "novel technologies for materials sensors and imaging" in 2010 from the same University. He is currently Senior Researcher with the Institute for Electromagnetic Sensing of the Environment (IREA) of the National Research Council of Italy (CNR). A primary focus of his work is the development optofluidic sensors based on Raman and fluorescence spectroscopy. Another part of his activity is aimed at the development of sensors based on optical waveguides, ranging from optical fiber sensors to polymer waveguides manufactured by photolithographic processes.

Romeo Bernini (Member, IEEE) received the Laurea degree (*summa cum laude*) from the University of Naples Federico II, Naples, Italy, and the Ph.D. degree in electronic engineering from the Second University of Naples, Aversa, Italy, in 1995 and 1999, respectively. He was a Research Fellow with the Second University of Naples in 2000. He is currently the Research Director with the Institute for the electromagnetic sensing of the environment (IREA) of the Italian National Research council (CNR). He has authored or coauthored more than 100 papers published in various international journals. His research interests include optoelectronic devices and sensors, microfluidic and optofluidic devices and fiber optic sensors. He is a Reviewer for several technical journals. He holds one international and two national patents on fiber optic sensors.